ADVANCED BIOLOGY
www.advanced-bio.com

SOX4 Regulates Thermogenesis in Brown Adipose Tissue via Independent Complexes with EBF2 and PPARγ

Shuai Wang, Ting He, Tong Fu, Yu Zhu, Yixin Wei, Wenlong Xie, Huanming Shen, Ya Luo, Boan Li, Huiling Guo,* and Weihua Li**

Brown adipose tissue (BAT) is crucial for maintaining whole-body metabolic homeostasis and combating obesity and metabolic disorders. SOX4 collaborates with EBF2 to promote the expression of thermogenic genes in BAT, but it is unclear whether there are mechanisms independent of this regulation. However, it is found that SOX4 can directly interact with the promoter regions of thermogenic genes, thereby activating their expression. Simultaneously, early B cell factor 2 (EBF2) and peroxisome proliferator-activated receptor-γ (PPARγ) can independently interact with SOX4, forming two distinct complexes that promote the expression of thermogenic genes. Phenotypically, the deletion of SOX4 in BAT of mice (*Ucp1*$^{Cre+}$-*Sox4*$^{f/f}$ (*Sox4-BKO*)) leads to the downregulation of thermogenic and oxidative phosphorylation genes, as well as a reduction in mitochondrial numbers. Furthermore, *Sox4-BKO* mice are more susceptible to obesity, glucose intolerance, and insulin resistance when subjected to a high-fat diet (HFD). Consistently, the loss of SOX4 results in increased cellular triglyceride content and reduced expression levels of thermogenic genes in vitro. Together, a novel mechanism by which SOX4 regulates thermogenesis in BAT is elucidated, offering a promising strategy to address obesity and metabolic disorders.

1. Introduction

Obesity, a pandemic disorder, raises the risks of type 2 diabetes, dyslipidemias, cardiovascular disease, nonalcoholic fatty liver disease (NAFLD), and other conditions, becoming one of the major clinical challenges of the 21st century.[1–4] Adipose tissue plays a critical role in the maintenance of metabolic homeostasis.[5] Generally, adipose tissue is classified into three distinct types: white adipose tissue (WAT), beige adipose tissue, and brown adipose tissue (BAT) in mammals.[6] WAT is primarily used to store excess energy, and its excessive accumulation leads to obesity and metabolic diseases.[7] In contrast, BAT is mainly involved in maintaining body temperature by consuming energy, while beige adipose tissue possesses characteristics of both WAT and BAT and can adapt to thermogenesis under certain conditions.[8,9] Activation of BAT is associated with accelerated lipid metabolism and improved insulin sensitivity, while deficiency of BAT exhibits "whitening" and reduces lipolysis, which makes mice susceptible to obesity.[10,11] Intensive studies have elucidated that human BAT activity is correlated with body weight.[12] Promoting BAT development and thermogenic function might prove to be a fascinating strategy to counteract obesity or metabolic disorders.[13–15]

BATs are packed with mitochondria, and uncoupling protein-1 (UCP1) is localized on the inner membrane of mitochondria.[16] UCP1 is activated and catalyzes the leak of protons to produce heat rather than ATP.[17] In response to cold, the sympathetic outflow to BAT is activated and then releases catecholamines, such as epinephrine and norepinephrine.[18,19] A large amount of catecholamines is

S. Wang, W. Li
Department of Cardiology
Xiamen Key Laboratory of Cardiac Electrophysiology
Xiamen Institute of Cardiovascular Diseases
The First Affiliated Hospital of Xiamen University
School of Medicine
Xiamen University
Xiamen 361003, China
E-mail: liweihua@xmu.edu.cn

S. Wang, T. He, T. Fu, Y. Zhu, Y. Wei, W. Xie, B. Li, H. Guo
State Key Laboratory of Cellular Stress Biology
Innovation Center for Cell Signaling Network and Engineering Research
Center of Molecular Diagnostics of The Ministry of Education
School of Life Sciences
Xiamen University
Xiamen, Fujian 361102, China
E-mail: bali@xmu.edu.cn; ghuiling@xmu.edu.cn

H. Shen
Shenzhen Institute of Advanced Technology
Chinese Academy of Science
Shenzhen 518055, China

Y. Luo
National Institute for Data Science in Health and Medicine
School of Medicine
Xiamen University
Xiamen, Fujian 361003, China

The ORCID identification number(s) for the author(s) of this article can be found under https://doi.org/10.1002/adbi.202500224

DOI: 10.1002/adbi.202500224

released, and they bind to β3-adrenergic receptors in BAT and activate protein kinase A (PKA), subsequently enhancing the thermogenic program of BAT.[20] PKA can activate hormone-sensitive lipase (HSL) and adipose triglyceride lipase (ATGL), enhancing lipolytic function of triglyceride, which leads to an increased release of free fatty acids (FFAs) for utilization by mitochondria, thereby regulating thermogenesis in BAT. Mitochondria play a crucial role in maintaining thermogenic functions of BAT, and PPARγ coactivator-1 alpha (PGC1α) regulates mitochondrial biogenesis and function.[21–23] The loss of PGC1α reduces mitochondrial density and energy expenditure, contributing to cold sensitivity and obesity in mice.[24]

Several transcriptional factors have been shown to regulate thermogenic function of BAT. PPARγ is highly expressed in BAT and necessary for the development of BAT, and PPARγ cooperates with PR-domain containing protein-16 (PRDM16) or PPARγ coactivator 1α (PGC1α) to promote brown adipogenesis and the expression of thermogenic genes.[25] The EBF2, a specific marker of brown preadipose cells and essential transcriptional regulator for brown fat cell fate, recruits PPARγ to brown fat-selective gene targets to maintain BAT identity.[11,26] Recent studies indicate that Ebf2 promotes the transcriptional activity of estrogen-related receptorα (ERRα) and PGC1α complex, leading to the upregulation of thermogenic genes in BAT.[27]

SOX4, which contains a high-mobility group DNA-binding domain (HMG-Box domain) and a C-terminal transactivation domain (TAD domain), plays a crucial role in regulating cell stemness, immune cell differentiation, and the development of the heart and the nervous system.[28–30] Recently, we found that SOX4 inhibits preadipocyte differentiation in iWAT through the Wnt pathway, and its overexpression converts preadipocytes into nonadipogenic lineages in vivo.[31] SOX4 also enhances beige adipocyte-driven adaptive thermogenesis by promoting the assembly of the PRDM16-PPARγ complex.[32] Our recent research found that the cooperation between SOX4 and EBF2 drives the transcription of thermogenic genes in brown adipocytes.[33] However, it remains unclear whether SOX4 regulates thermogenesis through other mechanisms.

In this study, we found that SOX4 directly binds to the promoter regions of thermogenic genes, activating their expression. SOX4 respectively cooperated with EBF2 and PPARγ to form two separate complexes, which further promoted the expression of thermogenic genes. We also found that early during brown adipocyte differentiation, SOX4 predominantly interacts with EBF2, while in later stages, SOX4 interacts predominantly with PPARγ. To further investigate the role of SOX4 in BAT, we crossed *Sox4*^{ff} mice with *Ucp1-cre* mice to generate BAT-specific knockout mice of SOX4 (*Sox4-BKO*). We found that depletion of SOX4 in BAT significantly reduced the expression of BAT-specific genes and oxidative phosphorylation genes. The loss of SOX4 predisposed mice to obesity, glucose intolerance, insulin resistance, and metabolic diseases on a high-fat diet (HFD). Interestingly, the ectopic overexpression of SOX4 in C2C12 or 3T3-L1 cells promoted the expression of thermogenic genes. These results indicated that SOX4 is crucial for regulating the thermogenic function of BAT, offering a novel strategy for treating obesity.

2. Results

2.1. SOX4 Cooperates with EBF2 and PPARγ to Promote the Expression of Thermogenic Genes

SOX4 has been suggested to act as a cofactor for PPARγ in regulating the thermogenic function of beige fat.[32] Additionally, SOX4 has been shown to associate with EBF2 to promote the expression of thermogenic genes in BAT.[33] Therefore, we further investigated whether SOX4 could form a transcriptional complex with EBF2 and PPARγ to enhance the expression of thermogenic genes in BAT. In the GEO database (GSE144490), the genes upregulated after rosiglitazone (PPARγ agonist) treatment of BAT showed an overlap of 17 genes with the down-regulated genes resulting from the knockout of SOX4 (GSE281236) and EBF2 (GSE144188) (**Figure 1A**). These overlapping genes included *Ucp1*, *Cidea*, and *Pparα* (Figure 1A). This indicates that SOX4 might cooperate with EBF2 and PPARγ to regulate thermogenesis of BAT. We then validated the interaction between endogenous PPARγ and SOX4 in lysates of mature brown adipocytes. As shown in Figure 1B, endogenous IP of SOX4 pulled down EBF2 and PPARγ. These results were further confirmed in 293T cells (Figure 1C). So far, there have been no reports of the interaction between EBF2 and PPARγ. We found that EBF2 did not co-immunoprecipitate with PPARγ in HEK293T cells (Figure 1D). Even upon overexpression of SOX4, the PPARγ protein was unable to interact with EBF2 protein (Figure 1E). A 2-step co-immunoprecipitation (co-IP) assay further demonstrated that SOX4 binds to EBF2 and PPARγ in independent complexes, rather than in a ternary complex involving all three proteins (Figure 1F–H). These data suggest that SOX4 forms two distinct complexes by interacting separately with EBF2 and PPARγ, rather than a ternary complex.

To further confirm whether the binding of SOX4 to EBF2 or PPARγ is differentiation stage-dependent, we first assessed the expression levels of SOX4, EBF2, and PPARγ on days 0 and 6 of differentiation. After 6 days of differentiation, *Sox4*, *Ebf2*, and *Pparγ* were progressively upregulated, with the most significant increase in *Pparγ* (**Figure 2A**). We further validated the interaction in BAT stromal vascular fraction (SVF) and mature brown adipocytes. The SOX4-PPARγ interaction is stronger in mature brown adipocytes than in BAT SVF, while SOX4-EBF2 interaction decreased (Figure 2B,C). We also conducted affinity assays in HEK293T cells and found that SOX4 exhibits a stronger binding affinity for PPARγ than for EBF2 (Figure 2D,E). With increasing levels of PPARγ, the interaction between SOX4 and PPARγ is markedly strengthened, while the association of SOX4 with EBF2 is correspondingly attenuated (Figure 2F). Collectively, SOX4 forms distinct complexes with PPARγ or EBF2, exhibiting a temporal interaction pattern.

To address the functional relationship between these proteins, we reanalyzed publicly available ChIP-Seq data (GSE263446, GSE97116, GSE144188). The −6 kb *Ucp1* enhancer and −25 kb *Prdm16* enhancer were occupied by SOX4, EBF2, and PPARγ in BAT (**Figure 3A,B**). The −6 kb *Ucp1* and −25 kb *Prdm16* enhancers, which contain putative SOX4 DNA binding sites, were cloned into a luciferase reporter construct. SOX4 alone

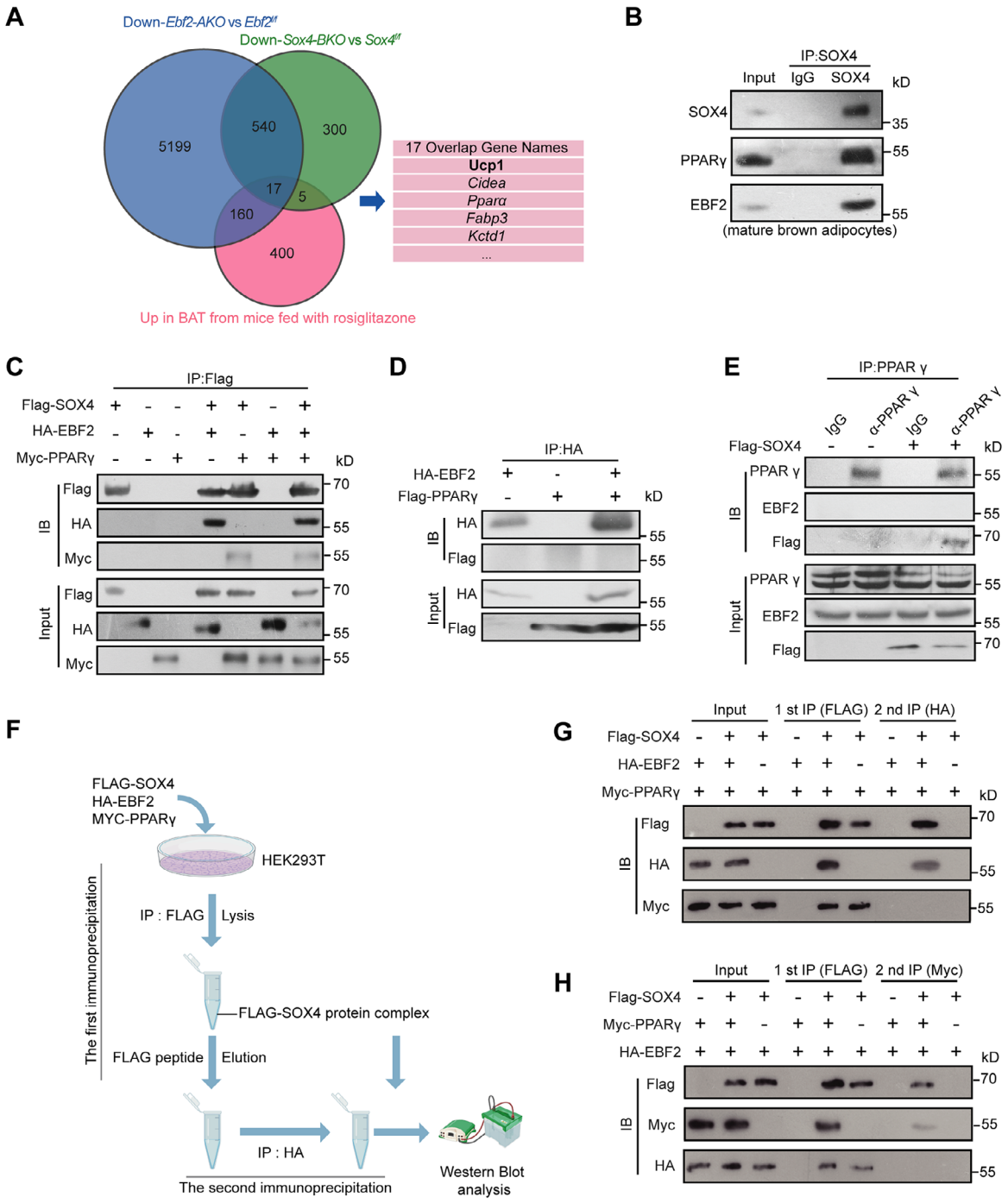

Figure 1. SOX4 respectively cooperates with EBF2 and PPARγ to form two separate complexes. A) Overlap (17) of genes down-regulated by SOX4 knockout, down-regulated by EBF2 knockout, and genes up-regulated in Rosig-treated classical BAT. B) BAT SVFs isolated from 3-week-old WT male mice were differentiated into brown adipocytes. On day 6, cells were harvested and lysed using IP lysis buffer. The lysates were subjected to immunoprecipitation with an anti-SOX4 antibody, followed by immunoblotting with anti-PPARγ, anti-EBF2, and anti-SOX4 antibodies. The interaction between endogenous SOX4 and EBF2 in mature brown adipocytes was used as a positive control. C) HEK293T cells were transfected with Flag-SOX4, HA-EBF2, or/and Myc-PPARγ as indicated and subjected to immunoprecipitation with anti-Flag. D) HEK293T cells were transfected with HA-EBF2 or/and Myc-PPARγ as indicated and subjected to immunoprecipitation with anti-HA. The input and pellet fractions were analyzed by western blotting. E) Overexpression of SOX4 in HEK293T cells failed to promote the interaction of EBF2 and PPARγ. F–H) Schematic diagram of two-step co-immunoprecipitation (F). HEK293T cells were transfected with FLAG–SOX4, HA–EBF2, and Myc–PPARγ. Immunoprecipitation was initially performed using an anti-FLAG antibody, followed by elution of the complex with FLAG peptide. A second round of immunoprecipitation was then carried out using an anti-HA antibody. Protein samples from each purification step were analyzed by western blot (G). HEK293T cells were transfected with FLAG–SOX4, HA–EBF2, and Myc–PPARγ. The first immunoprecipitation was performed with an anti-FLAG antibody. The complex was eluted with the FLAG peptide, followed by the second step of immunoprecipitation with an anti-Myc antibody. Protein samples from each step were subjected to Western blot analysis (H).

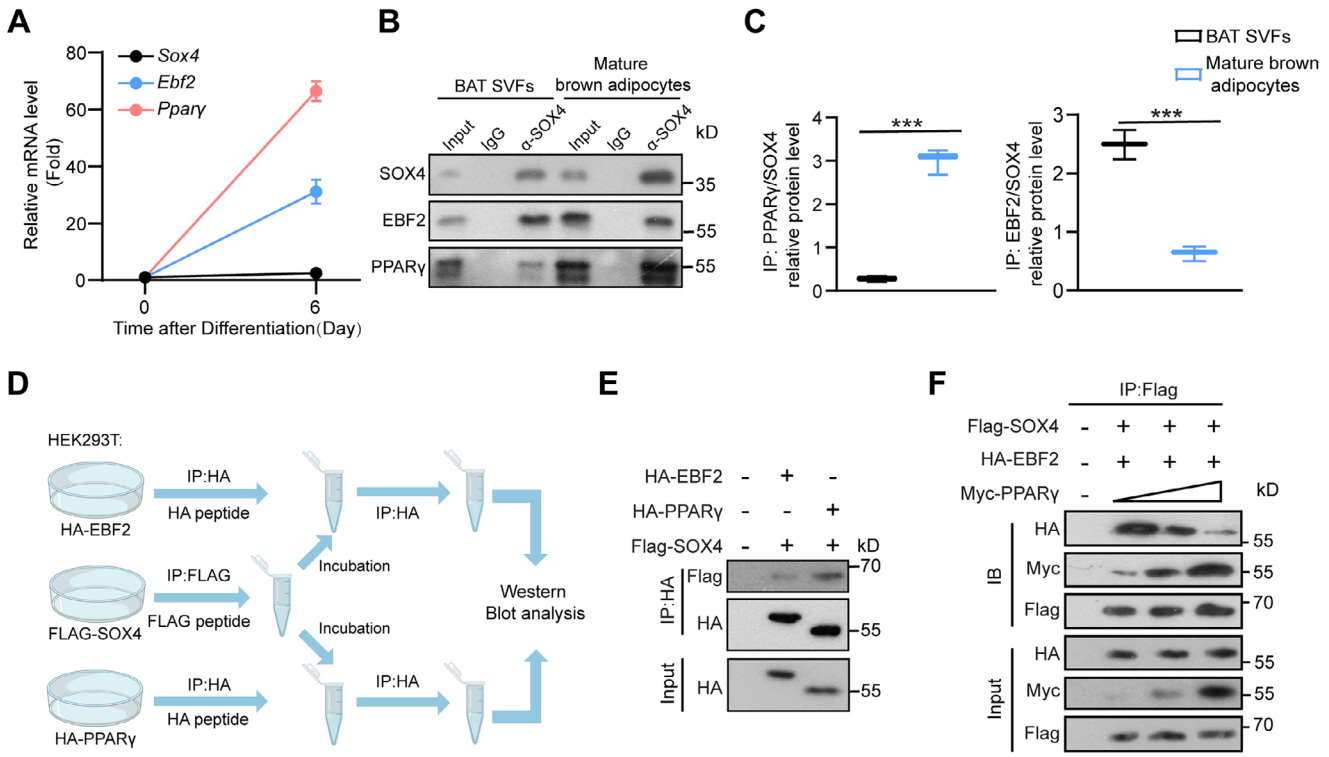

Figure 2. SOX4 forms distinct complexes with PPARγ and EBF2 in a temporal pattern. A) mRNA levels of *Sox4*, *Ebf2*, and *Pparγ* in brown adipocytes on days 0 and 6 of differentiation. *18S* was used as an invariant control. The mRNA levels in control mice were normalized to 1.0. B) BAT SVFs and differentiated brown adipocytes were harvested and lysed using IP lysis buffer. The lysates were subjected to immunoprecipitation with an anti-SOX4 antibody, and immunoblotting was performed with antibodies against PPARγ, EBF2, and SOX4. C) The relative protein levels of PPARγ/EBF2 to SOX4 in the IP group were quantified using ImageJ software. The SOX4 protein in the BAT SVFs of the IP group is localized at position 1. D,E) 293T cells were transfected with either HA-EBF2 or HA-PPARγ. After 48 h, the cells were collected, and the proteins were enriched using HA-conjugated beads and subsequently eluted with HA peptide. In parallel, 293T cells were transfected with FLAG-SOX4, collected after 48 h, and enriched with FLAG-conjugated beads, followed by elution with FLAG peptide. The eluted fraction from the FLAG beads was then divided equally and incubated with the HA-EBF2 and HA-PPARγ samples overnight at 4 °C. The resulting complexes were captured using HA beads and analyzed by western blotting. F) 293T cells were transfected with Flag-SOX4, HA-EBF2, and varying doses of Myc-PPARγ. After 48 h, the cells were collected, and proteins were enriched using FLAG beads. Both the input and elution fractions were analyzed by western blotting. Asterisks (*) denote the level of statistical significance. ***$p < 0.001$. Data are presented as mean ± SEM. Statistical analyses were determined by unpaired two-tailed Student's *t*-test (F).

exhibited ≈5-fold activation, whereas EBF2 or PPARγ alone failed to activate transcription of *Ucp1* (Figure 3C). Furthermore, co-overexpression of SOX4 and EBF2 resulted in ≈40-fold activation of *Ucp1*, while co-overexpression of SOX4 and PPARγ led to ≈10-fold activation (Figure 3C). The highest activation (≈90-fold) was observed with the co-expression of SOX4, EBF2, and PPARγ (Figure 3C). The activation pattern of SOX4, EBF2, and PPARγ on *Prdm16* mirrored that observed for *Ucp1* (Figure 3D). These findings suggest that SOX4 forms distinct complexes with EBF2 and PPARγ, together enhancing the expression of thermogenic genes.

2.2. SOX4 Directly Regulates the Transcription of Thermogenic Gene

Since SOX4 can independently activate the expression of thermogenic genes, including *Ucp1* and *Prdm16*, we further investigated whether SOX4 can directly regulate their transcription. As shown in Figure S1A,B (Supporting Information), overexpression of SOX4 in mature brown adipocytes significantly promoted the expression of thermogenic genes, including *Ucp1*, *Prdm16*, and *Pgc1α*. Based on these findings, we speculate that SOX4 might directly regulate the transcription of thermogenic genes. We reanalyzed publicly available ChIP-seq datasets (GSE263446) to determine whether SOX4 directly binds to the promoters of thermogenic genes. As shown in Figure S1C (Supporting Information), the promoter regions of *Ucp1*, *Prdm16*, *Pgc1α*, *Dio2*, *Cox8b*, and *Cidea* were bound by SOX4. The ChIP-qPCR assays confirmed the specific binding of SOX4 to the promoter regions of *Ucp1*, *Prdm16*, and *Pgc1α* (Figure S1D, Supporting Information). Meanwhile, we cloned fragments containing the −6 kb region of the *Ucp1* enhancer, the −1 kb region of the *Prdm16* promoter, or the −5 kb region of the *Pgc1α* genomic sequence, each containing a consensus SOX4-binding site (AACAAAG), into the luciferase reporter cassette. As shown in Figure S1E–G (Supporting Information), overexpression of SOX4 led to enhanced luciferase activity in the wild-type luciferase reporter. In contrast, mutation of the SOX4-binding site markedly reduced luciferase activity induced by SOX4 (Figure S1E–G, Supporting Information).

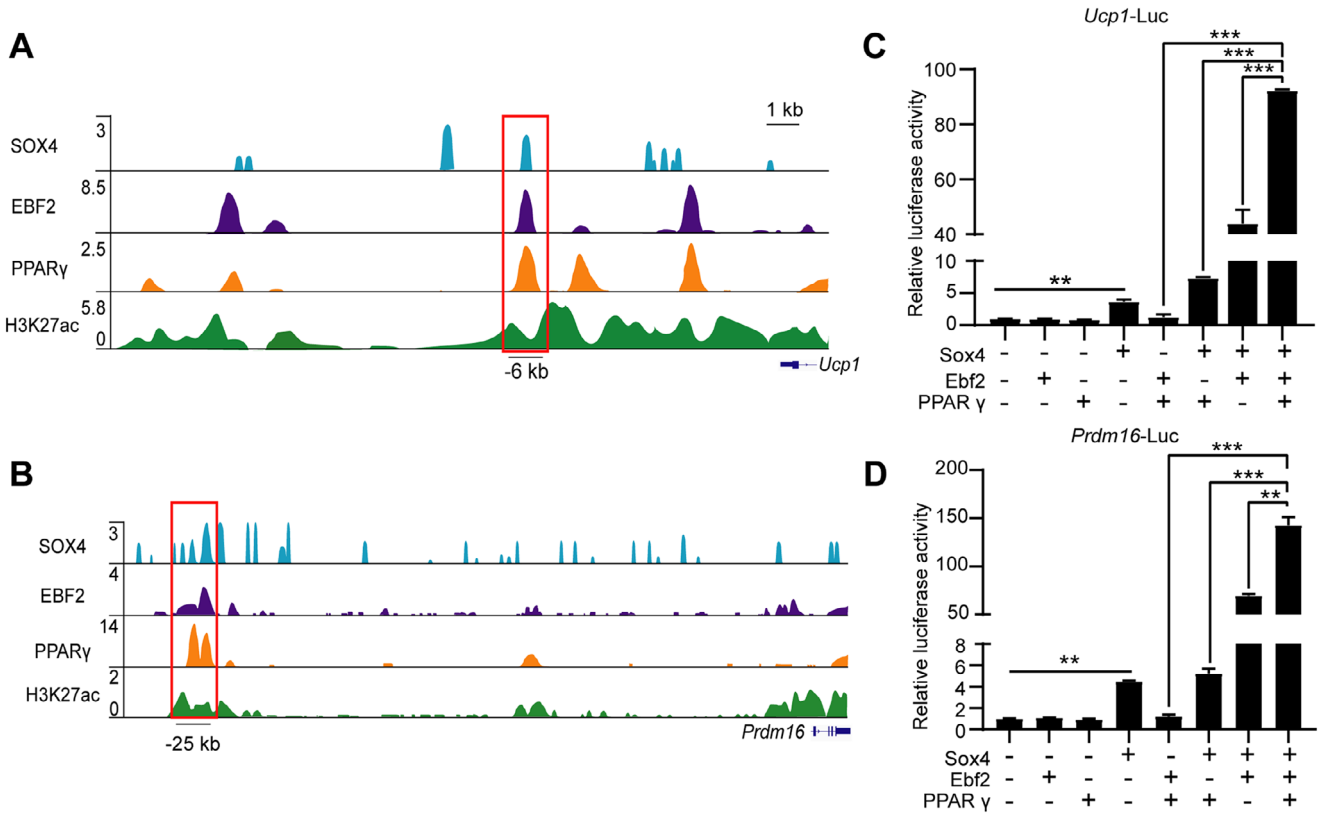

Figure 3. SOX4 cooperates with EBF2 and PPARγ to promote the expression of thermogenic genes. A,B) Representative binding profiles of SOX4, EBF2, PPARγ, and H3K27ac on *Ucp1* and *Prdm16*. C,D) Transcriptional activity of *Ucp1* −6 kb enhancer or *Prdm16* −25 kb in NIH 3T3 cells upon expression of Sox4, PPARγ, and EBF2 ($n = 3$). Asterisks (*) denote the level of statistical significance. $^{**}p < 0.01$, $^{***}p < 0.001$. Data are presented as mean ± SEM. Statistical analyses were determined by one-way ANOVA followed by Tukey's test (E,F).

PGC-1α, a key regulator of mitochondrial biogenesis and thermogenesis in BAT, is crucial for UCP1 expression and cold tolerance. Loss of PGC-1α impairs mitochondrial function and increases obesity susceptibility.[23,34,35] To further confirm the transcriptional regulatory role of SOX4 on *Pgc1α*, we performed a ChIP assay after overexpressing FLAG-SOX4 in differentiated brown adipocytes. SOX4 binds to ≈5 kb region of *Pgc1α* (Figure S2A, Supporting Information). To clarify whether the transcriptional activation of PGC1α depends on the HMG-box domain (HMG-BOX DNA-binding domain) or the TAD domain (C-terminal transactivation domain) of the SOX4 protein, we conducted luciferase assays using two mutants of SOX4 (ΔHMG and ΔTAD).[33] The results from luciferase assays indicated that the absence of either the HMG-box domain (ΔHMG) or the TAD domain (ΔTAD) failed to activate PGC1α-luciferase activity (Figure S2B, Supporting Information). Additionally, FAIRE-qPCR assays demonstrated that the loss of SOX4 significantly reduced chromatin accessibility at the *Pgc1α* enhancer (Figure S2C, Supporting Information). These findings suggest that SOX4 directly activates *Pgc1α* transcription.

2.3. SOX4 is Essential for the Expression of Thermogenic Genes In Vitro

To elucidate the role of SOX4 in the late-stage differentiation of brown adipocytes, we isolated BAT SVFs from 3-week-old *Sox4-BKO* mice and control littermates, and induced differentiation into brown adipocytes (**Figure** 4A). As shown in Figure 4B, the SOX4-knockout cells exhibited much higher triglyceride (TG) content than control cells. qPCR analysis showed that deletion of Sox4 severely attenuated the expression of thermogenic genes, including *Prdm16, Ucp1, Pgc1α, Cidea, Cox8b,* and *Ebf2* (Figure 4C). Consistent with the gene expression profiling, UCP1 and other thermogenic protein levels were lower in *Sox4-BKO* cells (Figure 4D). The decreased expression of PGC1α in *Sox4-BKO* cells prompted us to investigate whether the loss of Sox4 also reduces the expression of mitochondrial oxidative phosphorylation genes and the mitochondrial number in mature brown adipocytes. Consistent with the reduced thermogenic genes, mitochondrial oxidative phosphorylation genes were also diminished (Figure 4E). The intensity of MitoTracker staining and markers of mitochondrial content (*Nd1, Nd2,* and *Nd4*) were also

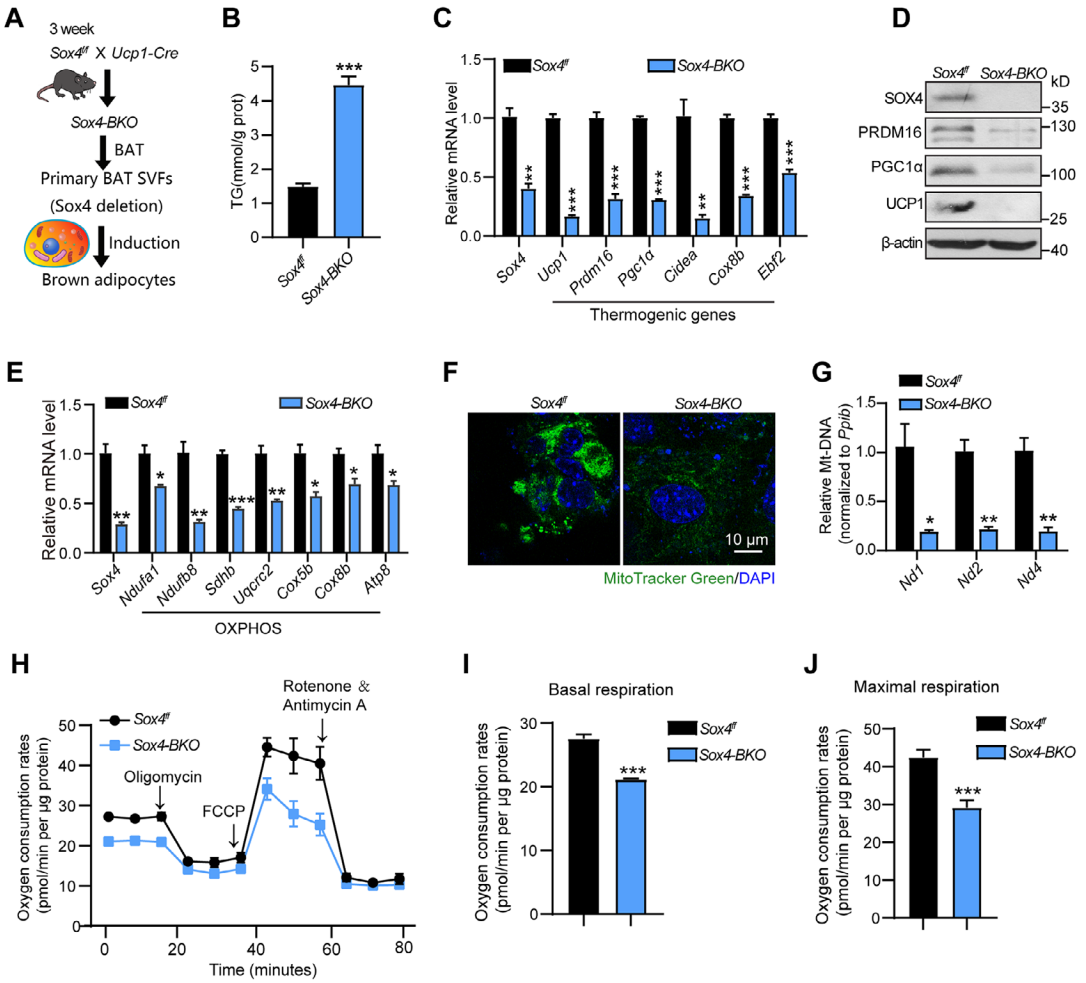

Figure 4. Sox4 plays a crucial role in the expression of thermogenic genes in vitro. A) BAT SVFs were directly isolated from 3-week-old *Sox4$^{f/f}$* and *Sox4-BKO* male mice and then subjected to differentiation. On day 6 of differentiation, the cells were harvested for a series of experiments. B) The TG content of the two groups of cells ($n = 3$). C,D) The RNA was extracted from the cells, and thermogenic genes and proteins were analyzed by qPCR (C) ($n = 3$) and western blot (D). *18S* was used as an invariant control. The mRNA levels in control cells were normalized to 1.0. E) The mRNA levels of mitochondrial oxidative phosphorylation genes in the two groups of cells ($n = 3$). *18S* was used as an invariant control. The mRNA levels in control cells were normalized to 1.0. F) The cells were subjected to MitoTracker Green staining. Scale bars, 10 μm. G) The DNA was extracted from the two groups of cells, mitochondrial-specific transcripts (*Nd1*, *Nd 2*, and *Nd4*) were determined by qPCR ($n = 3$). *Ppib* was used as an invariant control. The DNA levels in control cells were normalized to 1.0. H–J) The OCR of differentiated primary brown adipocytes is shown in (H), while the basal and maximal respiration rates are presented in (I,J), respectively ($n = 3$). Asterisks (*) denote the level of statistical significance. *$p < 0.05$, **$p < 0.01$, ***$p < 0.001$. Data are presented as mean ± SEM. Statistical analyses were determined by unpaired two-tailed Student's *t*-test (B,C,E,G,I,J).

markedly reduced in *Sox4-BKO* cells (Figure 4F,G). Consistently, SOX4-knockdown cells exhibited reduced basal mitochondrial respiration and diminished maximal mitochondrial respiratory capacity (Figure 4H–J). Furthermore, we established an immortalized BAT SVFs cell line, which further confirmed the above results (Figure S3A–F, Supporting Information). Collectively, these results indicate that Sox4 is crucial for the activation of the thermogenic gene program in vitro.

2.4. SOX4 is Indispensable for Expression of Thermogenic Genes In Vivo

Given that SOX4 can directly activate the expression of thermogenic genes, we further investigated whether the knockout of SOX4 in mature brown adipocytes would reduce the expression of thermogenic genes in vivo. We crossed *Sox4$^{f/f}$* mice with *Ucp1-Cre* mice to generate BAT-specific SOX4 knockout mice (referred to as *Sox4-BKO* mice), in which SOX4 was predominantly depleted in BAT (Figure S4A,B, Supporting Information). Our results indicated that the protein levels of SOX11 and SOX12, the other two key members of the SOXC family, remained unchanged (Figure S4A,B, Supporting Information). Furthermore, there was no difference in body temperature between *Sox4$^{f/f}$* and *Sox4-BKO* mice, while the surface temperature of *Sox4-BKO* mice was notably lower compared to the control group during acute cold stimulation (Figure S4C,D, Supporting Information). Consistent with our previous research, *Sox4-BKO* mice exhibited increased lipid accumulation in BAT compared to the controls (Figure S4E, Supporting Information).

Immunohistochemical analyses further indicated that *Sox4-BKO* mice exhibited significantly decreased UCP1 expression compared to controls (Figure S4E, Supporting Information). To gain insight into the function of SOX4 in BAT, the BAT of *Sox4-BKO* mice and littermate controls were subjected to RNA sequencing (RNA-Seq). Among the 10 731 genes identified as "expressed" by RNA-seq, the ablation of Sox4 resulted in the upregulation of 395 genes and the downregulation of 172 genes (**Figure 5**A). KEGG pathway analysis of the downregulated genes revealed that these genes were involved in thermogenesis, mitochondrial oxidative phosphorylation, TCA cycle, fatty acid degradation, and fatty acid metabolism (Figure 5B). Given the identified association of Sox4 with thermogenic genes, we performed additional KEGG pathway analyses focusing specifically on cellular metabolic pathways. As shown in Figure S5A,B (Supporting Information), downregulated cellular metabolic genes are predominantly enriched in fatty acid β-oxidation, triglyceride metabolism, and pyruvate metabolism, while upregulated genes are enriched in fatty acid synthesis, cholesterol synthesis, and fatty acid elongation. qPCR analysis revealed that the expression of thermogenic genes, including *Prdm16*, *Ucp1*, *PGC1α*, *Cidea*, *Elovl3*, *Dio2*, and *Ebf2*, was significantly reduced in the BAT of *Sox4-BKO* mice (Figure 5C). However, the expression of WAT-specific genes, including *Retn*, *Lyz2*, and *Agt*, was significantly upregulated (Figure 5D). These findings were further validated by western blot and immunofluorescence assays (Figure 5E,F). Given that Sox4 deletion reduces the expression of the mitochondrial oxidative phosphorylation genes and decreases mitochondrial number in vitro, we further investigated whether Sox4 loss affects mitochondrial oxidative phosphorylation genes and mitochondrial mass in vivo. In the BAT of *Sox4-BKO* mice, the mRNA levels of mitochondrial oxidative phosphorylation-related genes, such as *Ndufb8*, *Sdhb*, *Uqcrc2*, *Cox5b*, and *Cox8b*, were notably decreased compared to those in the control group (Figure 5G). Consistently, the levels of mitochondrial complex proteins were substantially reduced in BAT from *Sox4-BKO* mice (Figure 5H). Moreover, quantitative analysis revealed a reduction in mitochondrial number in BAT from *Sox4-BKO* mice (Figure 5I).

In line with the whitening phenotype observed in BAT,[33] the expression of the lipolysis-related genes such as HSL, ATGL, and MGLL was significantly downregulated in *Sox4-BKO* mice (Figure S6A,B, Supporting Information). Previous studies have suggested that BAT "whitening" promotes inflammation and lipogenesis in BAT.[36,37] We then reanalyzed the RNA-seq results and focused on the upregulated genes. Heatmaps revealed upregulation of numerous genes involved in inflammation, including *Il6*, *Il16*, *Tlr7*, *Ccl5*, and *Ccr7*, as well as lipogenesis, including *Fasn*, *Fads1*, *Acss2*, and *Scd1* (Figure S6C, Supporting Information). These findings were further validated by qPCR (Figure S6D,E, Supporting Information). Collectively, these results indicate that the loss of Sox4 reduces the expression of thermogenic genes while enhancing the expression of genes associated with lipogenesis and inflammation.

2.5. BAT-Specific SOX4 Knockout Predisposes Mice to Obesity and Metabolic Diseases Under HFD

To investigate whether the downregulation of lipolytic genes and the upregulation of lipogenic genes affect the overall metabolism of mice, we subjected the mice to chow diet (NCD) or HFD. On chow diet, there was no difference in body weight and indicated tissue weight between two groups (**Figure 6**A; Figure S7A, Supporting Information). Further experiments indicated that there were no significant differences in tissue size and lipid droplet accumulation between the groups (Figure S7B, Supporting Information). Metabolic cage analysis showed that oxygen consumption and heat production were similar with unchanged food intake and activity levels (Figure S7C–F, Supporting Information). We investigated whether the absence of SOX4 in BAT contributes to obesity under HFD. As shown in Figure 6A, *Sox4-BKO* mice exhibited faster weight gain compared to $Sox4^{f/f}$ mice. Moreover, *Sox4-BKO* mice exhibited more pronounced glucose intolerance and insulin resistance compared to the control group (Figure 6B,C). Analysis of body composition revealed an increase in fat mass, with no significant change in lean body mass in *Sox4-BKO* mice compared to controls (Figure 6D). Additionally, the mass of BAT, inguinal WAT (iWAT), gonadal WAT (gWAT), and the liver was markedly higher in *Sox4-BKO* mice compared to controls (Figure 6E), and we observed increases in the size of individual fat pads and livers (Figure 6F). Consistently, H&E staining showed enlarged lipid droplets in BAT, iWAT, and gWAT of *Sox4-BKO* mice and increased lipid accumulation in liver tissue (Figure 6F). As expected, *Sox4-BKO* mice exhibited increased levels of TG and free fatty acid (FFA) (Figure 6G,H). To further confirm that *Sox4-BKO* mice exhibited decreased metabolic parameters, we monitored their oxygen consumption and heat production using a metabolic cage system. HFD-fed *Sox4-BKO* mice exhibited markedly lower oxygen consumption and heat production, with food intake and locomotor activity remaining similar to $Sox4^{f/f}$ mice (Figure 6I–L). These observations indicate that deletion of SOX4 in BAT impairs whole-body metabolism and accounts for metabolic diseases.

2.6. SOX4 Stimulates the Expression of Thermogenic Genes in Nonbrown Adipocyte Lineages

To investigate whether SOX4 alone can initiate the expression of thermogenic genes, we overexpressed SOX4 in 3T3-L1 cells via lentivirus on the fourth day of differentiation. On day 8 of differentiation, cells overexpressing SOX4 exhibited much lighter Oil Red O staining compared to control cells, indicating a significant reduction in intracellular TG levels (Figure S8A,B, Supporting Information). As expected, overexpression of SOX4 markedly increased the expression of thermogenesis-related genes (Figure S8C, Supporting Information). Lineage tracing studies have demonstrated that BAT depots originate from precursor cells expressing *Myf5*, which are also shared with skeletal muscle in vivo.[38] We overexpressed SOX4 in muscle precursor cells (C2C12) using lentivirus and analyzed the

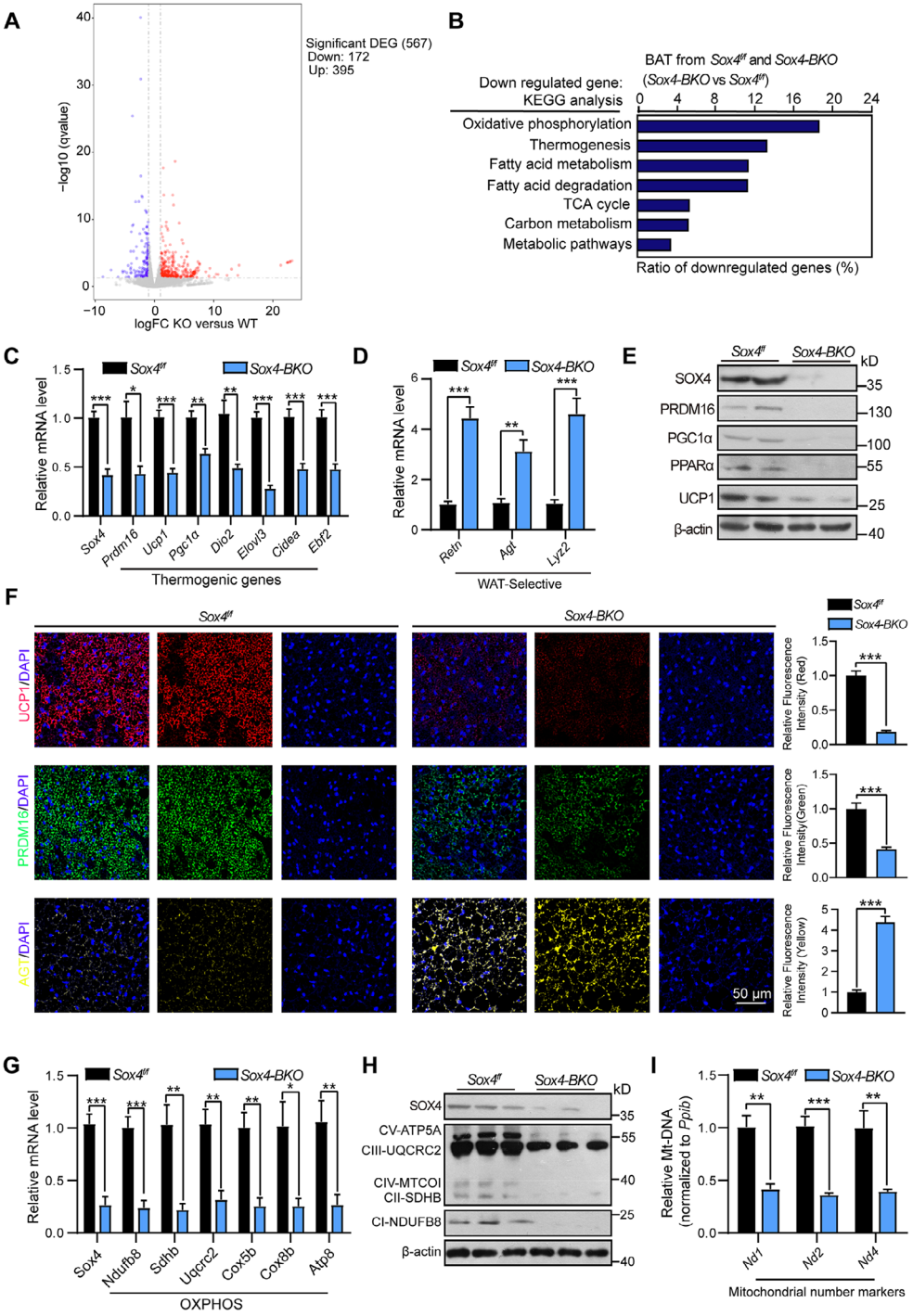

Figure 5. Sox4 is essential for the expression of thermogenic genes in vivo. A,B) The BATs from 8-week-old male mice were subjected to RNA-Seq. A volcano plot displaying the significance of genes differentially expressed in BAT of *Sox4-BKO* mice compared to control mice (A). The downregulated genes were conducted KEGG analysis (B). C,D) The mRNA levels of thermogenic genes (C) and WAT-selective genes (D) in BAT from 8-week-old *Sox4*$^{f/f}$ and *Sox4-BKO* male mice ($n = 4$). E) The protein levels of SOX4, PRDM16, UCP1, PPARα, and PGC1α in BAT. F) Immunofluorescence analysis showing UCP1 (top), PRDM16 (middle), and AGT (bottom) expression in BAT (left panel). Scale bars, 100 μm. Relative fluorescence intensity was quantified using ImageJ software (right panel). G) The mRNA levels of mitochondrial oxidative phosphorylation-related genes in BAT from 8-week-old *Sox4*$^{f/f}$ and *Sox4-BKO* male mice ($n = 4$). *18S* served as an invariant control, and the mRNA levels in control mice were normalized to 1.0. H) Western blot analysis of mitochondrial respiratory chain components in BAT from 8-week-old male *Sox4-BKO* and control mice ($n = 3$). I) Mitochondrial-specific transcripts (*Nd1*, *Nd2*, and *Nd4*) were quantified by qPCR in BAT mitochondrial DNA (mt-DNA) from BAT of 9-week-old *Sox4-BKO* and control male mice ($n = 4$). *Ppib* served as an invariant control, and the DNA levels in control mice were normalized to 1.0. Asterisks (*) denote the level of statistical significance. $*p < 0.05$, $**p < 0.01$, $***p < 0.001$. Data are presented as mean ± SEM. Statistical analyses were determined by unpaired two-tailed Student's *t*-test (C,D,G,I).

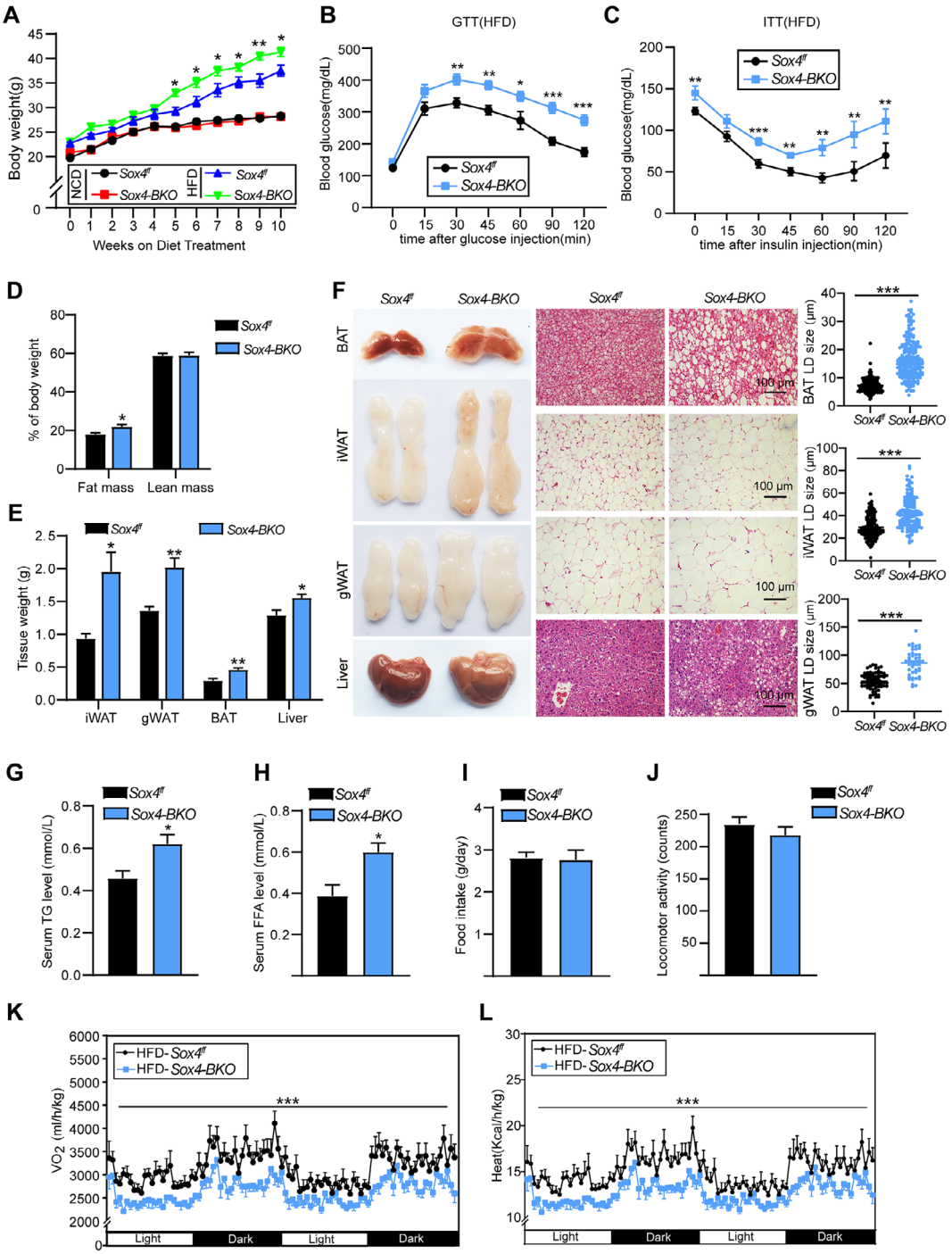

Figure 6. SOX4 deficiency increases susceptibility to obesity and metabolic disorders. A) *Sox4*$^{f/f}$ and *Sox4-BKO* male mice (6-week-old, $n = 6$) were subjected to chow, or high-fat diet (HFD) feeding. Body weights were monitored every week. B) On week 10, the mice were fasted for 16 h followed by an intraperitoneal injection of D-glucose (1.5 mg kg^{-1}) for GTT. Blood glucose levels were subsequently measured from the tail vein at indicated time points ($n = 5$). C) On week 11, the mice underwent a 6-h fasting period and were then intraperitoneally injected with insulin at a dose of 1 U kg^{-1} for ITT. Blood glucose levels were measured from the tail vein at specified time points ($n = 5$). D) On week 9, the average fat and lean mass of mice were quantified using the Echo MRI composition analyzer ($n = 5$). E) On week 11, mice were sacrificed. The representative ratios of tissue weight/body weight ($n = 5$). F) The tissue appearance and H&E staining (left panel) were shown. Scale bars, 100 μm. The diameters of lipid droplets (LD) in the H&E staining images were measured using ImageJ software (right panel). G,H) Serum levels of triacylglycerol (TG) (G) and free fatty acid (FFA) (H) were assessed ($n = 5$) at 11 weeks. I–L) On week 11, the mice were subjected to metabolic cage analysis. Food intake (I), locomotor activity (J), oxygen consumption (K), and heat production (L) of mice were measured in 2 consecutive days ($n = 6$). Asterisks (*) denote the level of statistical significance. *$p < 0.05$, **$p < 0.01$, ***$p < 0.001$. Data are presented as mean ± SEM. Statistical analyses were determined by unpaired two-tailed Student's *t*-test (A–E,G–L) and unpaired two-tailed Mann–Whitney test (F, right panel).

expression of the brown preadipose marker genes. Overexpression of SOX4 was sufficient to drive the expression of brown preadipose-selective genes, including *Sfrp4*, *Ren1*, *Meox1*, and *Fam129a* (Figure S8D, Supporting Information). Next, we treated C2C12 cells with adipogenic inducers and analyzed the expression of thermogenic genes. As shown in Figure S8E (Supporting Information), ectopic expression of SOX4 significantly activated the expression of thermogenic genes, including *Ucp1*, *Ebf2*, *Cidea*, and *Prdm16*. These results suggest that SOX4 promotes the differentiation of non-brown adipocyte lineages into brown adipocytes.

3. Discussion

SOX4 plays such a significant role in thermogenesis, and the deficiency of SOX4 causes mice to develop hypothermia under acute cold stress.[32] EBF2 maintains BAT identity by recruiting PPARγ to its brown-selective binding sites.[11] SOX4 effectively promotes the transcription of EBF2 and works together with EBF2 to further stimulate the expression of thermogenic genes.[33] However, it remains uncertain whether any thermogenic pathways exist that do not depend on EBF2. Forskolin, a potent adenylate cyclase activator, increases intracellular cAMP levels and activates the protein kinase A (PKA) signaling pathway, mimicking cold stimulation and leading to SOX4 phosphorylation and its translocation into the nucleus.[39] Here, we found that the absence of SOX4 inhibited the activation of thermogenic genes induced by the PKA signaling pathway. Interestingly, ectopic overexpression of SOX4 in C2C12 or 3T3-L1 cells stimulated the expression of thermogenic genes. ChIP-Seq analysis and luciferase assays further confirmed that SOX4 directly regulated the expression of thermogenic genes. Furthermore, there have been no reports of EBF2 forming a transcriptional complex with PPARγ. We found that EBF2 and PPARγ proteins cannot form a complex, indicating that SOX4 cooperated with EBF2 and PPARγ separately to form two distinct transcriptional complexes. Despite this separation, these two complexes synergistically enhance the activation of thermogenic genes (**Figure 7**). The SOX4-EBF2 and SOX4-PPARγ complexes play crucial roles in maintaining the identity of brown adipocytes. SOX4, EBF2, and PPARγ exhibit highly similar binding sites on the promoters of thermogenic genes. We hypothesize that the SOX4-EBF2 complex initially binds to the promoter regions of thermogenic genes to open chromatin, followed by the binding of the SOX4-PPARγ complex to further promote the expression of these genes. The interaction between SOX4, EBF2, and PPARγ plays a pivotal role in maintaining energy homeostasis in thermogenic adipose tissue. In beige fat, while the loss of SOX4 does not affect PPARγ expression levels, it significantly diminishes the interaction between PRDM16 and PPARγ. This disruption leads to cold intolerance and reduced expression of thermogenic genes in mice.[32] In BAT, SOX4 deficiency directly suppresses EBF2 expression, impairing the SOX4-EBF2 signaling pathway and weakening thermogenesis. As a result, the mice become more susceptible to obesity and metabolic disorders when subjected to a high-fat diet.[33]

BAT also plays a significant role in energy expenditure, and the defects in BAT function could lead to obesity and related

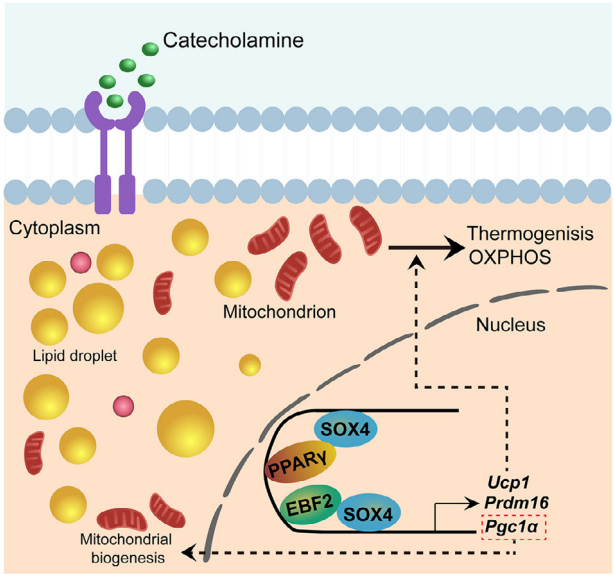

Figure 7. Schematic diagram summarizing the working model of SOX4 in regulating BAT thermogenesis. SOX4 can directly bind to the promoters of thermogenic genes and activate their expression. Additionally, both EBF2 and PPARγ can interact with SOX4, forming distinct complexes that further enhance expression of thermogenic genes in BAT.

metabolic disorders in mammals. PPARγ, highly expressed in BAT and essential for the development of BAT, drives the thermogenic program by interacting with co-activators and regulators, such as PGC-1α and PRDM16.[40] PRDM16, which lacks the ability to bind DNA, acts as a transcriptional cofactor that associates with PPARγ after it binds to the promoter region of thermogenic genes, facilitating the expression of these genes.[13,41] PGC-1α can directly bind to the promoter regions of thermogenic genes to enhance their expression. Additionally, PGC-1α functions as a coactivator, binding to PPARγ to further augment its activation of thermogenic gene expression.[42] Recently, we found that in beige fat, SOX4 can promote thermogenesis by enhancing the interaction between PPARγ and PRDM16, which is highly significant for the treatment of obesity.[32] Thus, we hypothesized that a deficiency of SOX4 in UCP1^{+} brown adipocytes could lead to obesity and metabolic defects. To test our hypothesis, we generated a mouse model with specific knockout of SOX4 in BAT (*Sox4-BKO*) by crossing *Ucp1-cre* mice with *Sox4*$^{f/f}$ mice. Unlike the *Myf5-Cre* and *Adiponectin-Cre* mouse models, *Ucp1-Cre* mice can relatively specifically target mature thermogenic adipose tissue. Although UCP1 expression is also found in specific neuronal populations in the hypothalamus, such as glutamatergic neurons in the VMH, we found that food intake in *Sox4-BKO* mice was not affected.[43] As expected, *Sox4-BKO* mice showed faster weight gain, increased glucose intolerance, insulin resistance on HFD, and increased tissue weight of iWAT, gWAT, and the liver. The increased tissue weight of iWAT, gWAT, and liver in *Sox4-BKO* mice may result from reduced lipolytic capacity in BAT, leading to the accumulation of excess triglycerides in these tissues. Due to the deficiency of brown adipose tissue thermogenic function, which leads to obesity and metabolic disorders, we further conducted RNA-Seq. Consistently, the loss of SOX4 in BAT resulted in the

downregulation of thermogenic, oxidative phosphorylation genes and lipolysis-related genes, and the upregulation of inflammation- and lipogenesis-associated genes. Alterations in the expression of these genes contributed to weakened lipid metabolism capacity of BAT, which made *Sox4-BKO* mice more prone to obesity and metabolic disorders under high-fat feeding conditions. Notably, the absence of SOX4 results in reduced expression of PRDM16. This suggests that SOX4 loss might indirectly destabilize the PRDM16 complex, thereby weakening the thermogenic gene program. However, it has not been investigated whether overexpression of SOX4 could treat obesity in *ob/ob* or DIO obese mice.

Mitochondrial biogenesis enhances energy expenditure and promotes heat production in brown adipocytes. Defects in mitochondrial biogenesis impede the sustained proliferation and differentiation of progenitors, leading to suppressed tissue growth and regeneration.[34,35] PGC-1α plays a pivotal role as a master regulator of mitochondrial biogenesis, and its loss results in reduced mitochondrial density and UCP-1 protein levels, contributing to cold sensitivity and obesity.[23,24,35] Our study revealed that the loss of SOX4 led to decreased PGC-1α expression and mitochondrial biogenesis in BAT. SOX4 directly binds to the promoter region of PGC1α and utilizes its HMG and TAD domains to activate transcription of PGC1α. Gene expression analysis demonstrated that SOX4 deletion led to a significant downregulation of mitochondrial oxidative phosphorylation genes. The reduced expression of PGC1α and mitochondrial oxidative phosphorylation genes resulted in the reduced thermogenic capacity in *Sox4-BKO* mice.

SOX4 is essential for regulating thermogenesis by directly modulating the expression of thermogenic genes. It forms two distinct complexes with EBF2 and PPARγ, which collectively enhance the expression of thermogenic genes. The absence of SOX4 in BAT results in reduced expression of both thermogenic and oxidative phosphorylation genes. Furthermore, *Sox4-BKO* mice exhibit an increased susceptibility to obesity and metabolic disorders on a HFD. These findings suggest that targeting SOX4 could offer a novel therapeutic strategy for managing obesity and metabolic disorders, underscoring its potential as a key regulator of metabolic health.

4. Experimental Section

Mice: All mouse experiments were approved by the Institutional Animal Care and Research Advisory Committee at Xiamen University. Mice were kept in colony cages under controlled conditions: temperatures range of 22–24 °C, humidity levels of 50–60%, and a 12-h light/dark cycle beginning at 7:00 am. All mice were age-matched males with a C57BL/6 genetic background, with specific ages detailed in the figure legends. *Sox4-BKO* mice with a C57BL/6J background have been previously described (GemPharmatech Company, Nanjing, China).[31] WT mice were obtained from the Shanghai Model Organisms Center. Genotyping was performed using Taq MasterMix (CWBIO, Cat#CW0690H), with the primers listed in Table S1 (Supporting Information) (Beijing Tsingke Biotech Co., Ltd.). The high-fat diet was provided by Readydietech Co., Ltd. (Shenzhen, P.R. China), while the normal chow diet was provided by Jiangsu Xietong Pharmaceutical Bio-engineering Co., Ltd. (Jiangsu, P.R. China). The chow diet comprises 67.4% carbohydrates, 20.6% protein, and 12% fat. In contrast, the high-fat diet consists of 20% of calories from carbohydrates, 20% from protein, and 60% from fat.

Cell Culture and Adipocyte Differentiation: C2C12 cells and 3T3-L1 cells were obtained from Pricella Life Science&Technology Co.,Ltd. BAT SVF cells were isolated from mouse BAT, as described previously.[10] Cells were maintained in a culture medium composed of high-glucose DMEM (SUNNCELL, Cat#SNM-002A), supplemented with 100 U mL^{-1} penicillin, 100 mg mL^{-1} streptomycin (Biochannel, Cat#BCCE007), 1 mM sodium pyruvate (BasalMedia, Cat#S410JV), 1% NEAA (IMMOCELL, Cat#IMC-D07), and 10% FBS (CellMax, Cat#SA201).

To differentiate mature brown adipocytes, BAT SVFs cells were cultured in 20% FBS (AMOBIO, Cat#FBSAB001) until they reached 90–95% confluence in 6-Well Plate+6 Inserts, 1 µm Pore Size PET (Polyester) Membrane (Wuxi NEST Biotechnology Co., Ltd, Cat#723431). Cells were then treated for 2 days with Medium A, which consisted of 1 nM T3 (Sigma–Aldrich, Cat#T2877), 0.125 mM indomethacin (Sigma–Aldrich, Cat#I7378), 1 ϵM rosiglitazone (GLPBIO, Cat#GC16444), 5 ϵM dexamethasone (Sigma–Aldrich, Cat#D1756), 850 nM insulin (MCE, Cat#HY-P0035), and 0.5 mM IBMX (Sigma–Aldrich, Cat#I5879). After 48 h, the cells were switched to Medium B, containing 1 nM T3, 1 ϵM rosiglitazone, and 850 nM insulin. The cells were maintained in Medium B with medium changes every 2 days until they were harvested. On day 7, the cells had differentiated into mature brown adipocytes for further assays.

Serum Analysis: Before euthanizing the mice, blood samples were collected from the eyeballs and centrifuged at 1800 g for 15 min at 4 °C (DRAGONLAB, Cat#DM0436E), then the supernatants were collected. The levels of triglycerides (TG) and free fatty acids (FFA) were measured by TG kit (Nanjing Jiancheng, Cat#A110-1-1) and FFA kit (Bioswamp, Cat#BTK026), respectively.

Immunohistochemistry and Immunofluorescence: For Hematoxylin and Eosin (H&E) staining, the specified tissues from euthanized mice were fixed in 4% PFA at room temperature overnight. The fixed tissues were dehydrated with ethanol, embedded in paraffin, and sectioned at a thickness of 4 µm. The sections were stained with H&E Staining Kit (Wanleibio, Cat#WLA051a) following the manufacturer's instructions.

For immunofluorescence, the antigen retrieval was performed using antigen retrieval solution (Keygen BioTECH, Cat#KGC3110). The slides were first treated with 3% BSA and 0.1% Triton X-100 (Yuanye) in PBS for 1 h at room temperature. Following the blocking step, then subjected to primary antibodies: anti-UCP1 (Biodragon, Cat#RM8227) (dilution 1:100), anti-PRDM16 (Abcam, Cat#ab106410) (dilution 1:50), and AGT (Abclonal, Cat#A11689) (dilution 1:100). Subsequently, the slides were treated with secondary antibodies labeled with fluorescent markers (EpiZyme) and then incubated in the dark at room temperature for 1 h. Next, the slides were stained with 5 µg mL^{-1} DAPI (Mei5 Biotech, Cat#MF681-plus-01) for 10 min. Finally, imaging was performed using the Zeiss LSM 980 confocal microscope.

For the immunohistochemical analysis, paraffin-embedded tissue sections were first deparaffinized using xylene and rehydrated through a graded ethanol series to distilled water. To enhance antibody binding, antigen retrieval was conducted by immersing the sections in citrate buffer (pH 6.0) and heating in a microwave for 10 min at high power, followed by cooling at room temperature for 20 min. The sections were then treated with 3% hydrogen peroxide (filtered through filter (Bioland, Cat#CS05-040)) for 10 min at room temperature to block endogenous peroxidase activity. Subsequently, permeabilization was achieved with 0.1% Triton X-100 for 15 min to improve antibody penetration. After blocking with 5% BSA (EXCellBio, Cat#FSP500) for 30 min at room temperature to minimize nonspecific binding, the sections were incubated with anti-UCP1 (Santa, Cat#sc-518171) (diluted at 1:200) overnight at 4 °C. Following three 5-min washes with PBS, the sections were incubated with a secondary antibody (ZCIBIO Technology, Cat#ZC-G2129), at a dilution of 1:5000 for 30 min at room temperature. The immunoreactivity was visualized using a DAB substrate kit (Elabscience, Cat#E-IR-R217) according to the manufacturer's instructions. The sections were counterstained with hematoxylin for 5 min to provide nuclear contrast, dehydrated through graded ethanol, cleared with xylene, and mounted with neutral resin for microscopic examination.

Body-Composition Analysis: Mice were immobilized and positioned in the Echo MRI Composition Analyzer (Echo Medical Systems, 100H) to measure fat mass and lean mass.

Glucose Tolerance Test and Insulin Tolerance Test: For the glucose tolerance test (GTT), indicated HFD mice were fasted for 16 h with access to water only, followed by an intraperitoneal injection of D-glucose (Aladdin) at 1.0 g kg^{-1} body weight. For the insulin tolerance test (ITT), mice were fasted for 6 h with access to water and then received an intraperitoneal injection of human insulin at 1.5 U kg^{-1}. Blood samples were taken from the tail vein at time points of 0, 15, 30, 45, 60, 90, and 120 min post-injection, and glucose levels were assessed.

Metabolic Cage Study: Prior to the experiment, mice were individually housed at 22 °C for 1 week, followed by a 2-day acclimation period in metabolic cages. The Sable Promethion System was used to record various parameters, including food consumption, body weight, oxygen usage, heat output, and movement activity.

Western Blot Analysis: The samples were lysed using RIPA buffer (APExBIO, Cat#K1120) with added phosphatase and protease inhibitors (TargetMol, Cat#C0001) and sonicated by an ultrasonic processor (SCIENTZ). The concentrations of protein were measured using a BCA assay (BOXBIO, Cat#AKPR017). Proteins were separated by SDS-PAGE (CYTOCH, Cat#PW0002) and then transferred to PVDF membranes at a constant current of 250 mA for 2 h (DLAB Scientific Co., Ltd, Cat#18901229). Membranes were blocked with Fastest Blocking Reagent (HYCEZMBIO, Cat# HYC00811) and incubated with primary antibodies: SOX4 (HUABIO, Cat#ER1916-97), PRDM16 (Abcam, Cat#ab106410), PGC1α (SAB, Cat#37818), EBF2 (Affinity, Cat#DF13398), UCP1 (Diagbio, Cat#db9840), PPARγ (Bioworld, Cat#BS79617), OXPHOS (Abcam, Cat#110413), SOX11 (ELK Biotechnology, Cat#ES11939), SOX12 (HUABIO, Cat#ER64999), Flag (Sigma–Aldrich, Cat#F7425), HA (Bioss, Cat#BMS0966M), PPARα (BOSTER, A00600-2), and β-actin (Sino Biological, Cat#109444-T36), HSL (ZENBIO, Cat#344379), ATGL (Abways, Cat#CY8408), MGLL (Abcepta, Cat#AP16876a). All antibodies were used at a dilution of 1:1000, except for β-actin, which was diluted to 1:20000. After incubation with HRP-Goat Anti-Mouse Secondary Antibody (ZUNYAN, Cat#ZYID001-0050) (dilution 1:5000) and HRP-Goat Anti-Rabbit Secondary Antibody (GenScript, Cat#A00098) (dilution 1:5000), proteins were visualized using enhanced chemiluminescence (Abbkine, Cat#BMU101).

Gene Expression Analysis: Total RNA was extracted using TRIzol reagent (Accurate Biology, Cat#AG21101) following standard protocols. cDNA synthesis was performed using a cDNA synthesis kit (Abm, Cat#G490) in PCR tube (Jet Biofil, Cat#PCR411200), and the gene expression were detected using a real-time PCR system (Bio-Rad) with SYBR Green (Yeasen, Cat#11201ES08). 18S mRNA served as the invariant control. Primer sequences are listed in Table S1 (Supporting Information).

For RNA-Seq, BAT tissues were collected from 8-week-old male *Sox4-BKO* mice and their control littermates ($n = 2$). Total RNA was extracted with RNAisoReagent (YoungGen, Cat#RP101A), and sequenced using the Illumina HiSeq2500 platform by GENWIZ (Suzhou, China), and analyses were conducted by GENE DENOVO platform.

Oil Red O Staining: The Oil Red O working solution (Solarbio, Cat#G1262) was preheated at 37 °C before the experiment. Cells were fixed with 4% formalin (Energy Chemical, Cat#M0113619) for 15 min at room temperature and stained with the Oil Red O working solution for 10 min in culture plates (CellPro Biotechnology, Cat#803006) coated with poly-L-lysine. Next, the samples were rinsed three times and examined to microscopic.

Plasmids, Virus Packaging, and Infection: To construct knockdown plasmids, shRNA sequences were inserted into the pLKO.1 vector. To construct overexpression plasmids, the CDS of the indicated gene was purified (YALI Biotech, Cat#YC48001-200) and inserted into the pLV-N-Flag/HA/Myc vectors using T4 DNA ligase (CUSABIO, Cat#CSB-YP355583EDZ, https://www.cusabio.com). Plasmids were extracted using a SPINeasy Plasmid Midiprep Kit (MP Biomedicals, Cat#116539025). To produce lentivirus, HEK293T cells (Pricella, Cat#CL-0005) were transfected with the target plasmid, pHR, and pVSV-G plasmids, following standard protocols and using a transfection reagent (AbBOX, Cat#KX0110055). After 48 h, lentivirus particles were collected and concentrated (Sartorius, Cat#VS15T42). On the fourth day of differentiation, cells were infected with lentivirus in medium containing 10 μg mL^{-1} polybrene (HUAYUN, Cat#HYP490). AAV-GFP and AAV-SOX4 were purchased from Taitool Bioscience C., Ltd, Shanghai. Primer sequences of plasmid cloning are listed in Table S1 (Supporting Information).

Mitochondria Quantity Analysis: The BATs were incubated overnight at 55 °C in a TNES digestion buffer (0.2 M NaCl, 0.1 M Tris, 5 mM EDTA, 0.4% SDS) (LABLEAD) containing 200 μg mL^{-1} proteinase K (SYNTHGENE, Cat#10221) within a centrifuge tube (SAINING Biotechnology, Cat#3031100). Subsequently, genomic DNA was then isolated by the addition of 6 M NaCl, followed by precipitation with 100% ethanol. For mitochondrial quantification, RT-PCR was performed to amplify specific coding genes for NADH dehydrogenase 1, 2, or 4 (*Nd1*, *Nd2*, or *Nd4*), with the cyclophilin (*Ppib*) gene used as a reference with UltraStart Universal SYBR qPCR Master Mix (EXONGEN, Cat#A411-01). The primer sequences are provided in Table S1 (Supporting Information).

Luciferase Reporter Assays: For the construction of the luciferase reporter plasmid, the promoter regions of *Ucp1* or *Prdm16* (Novoprotein, Cat#NR005) were amplified from mouse genomic DNA and cloned into the pGL3-basic or pGL4.26 plasmid (Promega). The indicated luciferase reporter plasmid, together with a β-galactosidase (β-gal) control plasmid and other designated plasmids, was transfected into the cells using the EZ-Trans transfection reagent (Shanghai Life-iLab Biotech, Cat#AC04L092). Cells were harvested 48 h after transfection for luciferase and β-galactosidase assays (Neobioscience, Cat#LAS106.10).

Oxygen Consumption Rate (OCR) Measurements of Brown Adipocytes: Cells were seeded into XFe96 cell culture microplates and subjected to differentiate. The XF96 Extracellular Flux Analyzer (Seahorse Bioscience) was used to detect indicated indicators. Prior to the OCR assessment, the culture medium was exchanged for growth medium (Inner Mongolia Wanrui Biotechnology Co., Ltd, Cat#KX-A1222), which was included with 25 mM glucose, 1 mM sodium pyruvate, and 2 mM glutamine (Keygen BioTECH). During the experiment, sequential injections of 4 μM oligomycin, 2.5 μM FCCP, and 1.5 ϵM rotenone/antimycin were administered into the microplate to measure uncoupled respiration, maximal respiration, and nonmitochondrial respiration, respectively. The OCR values were then adjusted according to the protein concentration in each sample.

Immunoprecipitation: Proteins were extracted from the specified cells using lysis buffer (ACE, Cat#BK0060-01. Following this, the cell lysates were used for immunoprecipitation with FLAG/HA Magnetic Beads (Biolinkedin, Cat#L-1011) at 4 °C for 5–6 h. The eluted fraction was subjected to western blot analysis using the appropriate antibodies.

Chromatin Immunoprecipitation Assay: Chromatin Immunoprecipitation (ChIP) assay was performed on brown preadipocytes transduced with lentiviral vectors encoding either pLV-Flag-empty or pLV-Flag-SOX4. After differentiation induction, cells were fixed with 1% PFA, lysed with lysis buffer (Jiangsu Aidisheng Biological Technology Co., Ltd, Cat#ADS0004S0). An ultrasonic processor (SCIENTZ, Cat#SCIENTZ08-IIIA) was used on ice to achieve DNA fragmentation within the range of 200–1000 base pairs. And incubated with antibodies or FLAG beads for DNA enrichment. The assay followed the manufacturer's protocol (GZSC Bio Co., Ltd, Cat#KT101), with DNA enrichment analyzed by qPCR and normalized to input DNA.

FAIRE Assay: The cells were first treated with 1% PFA at ambient conditions for 10 min. Following fixation, the cells were lysed with SDS buffer for 10 min in centrifuge tubes (PakGent). The DNA within the lysates was then sheared to fragments ranging from 200 to 1000 base pairs using sonication. After centrifugation, the supernatant was incubated with RNase A at 37 °C for 1 h to eliminate RNA impurities. The samples were subsequently divided into two categories: one for de-crosslinking and one for maintaining the crosslinked state. For the de-crosslinking group, Proteinase K (Shanghai huding Biotech Co., Ltd., Cat#DYC-300103) was added and the samples were incubated overnight at 37.5 °C, followed by a 6-h incubation at 65 °C to ensure thorough de-crosslinking. Both sets of samples were purified using phenol-chloroform extraction. Chromatin accessibility was evaluated by qPCR using the FAIRE-PCR protocol, with primers specified in Table S1 (Supporting Information) (U&G Biotec, Cat#Q1002A).

Quantification and Statistical Analysis: Statistical analyses were conducted using GraphPad Prism 8.0 software and presented as mean ± SEM. Each dataset was assessed for normality using the Anderson-Darling, D'Agostino-Pearson, Shapiro–Wilk, or Kolmogorov–Smirnov tests, as appropriate. For comparisons between two groups, an unpaired two-tailed Student's *t*-test or unpaired two-tailed Mann–Whitney test was performed to evaluate statistical significance. Multiple group comparisons were conducted using the one-way/two-way ANOVA followed by Tukey's test, as specified in the figure legends. Quantitative analysis of immunofluorescence and lipid droplet size was performed using ImageJ software (National Institutes of Health). The lipid droplets were identified based on their distinct staining and morphology. The diameter of each lipid droplet was then measured using the measurement tools in ImageJ, with the diameter values expressed in micrometers (μm). The immunofluorescence quantification of UCP1, PRDM16, and AGT fluorescence intensity in the BAT of *Sox4*^{ff} mice was identified as 1. Details of the age and number of mice are provided in the figure legends. Significance levels are denoted as $*p < 0.05$, $**p < 0.01$, $***p < 0.001$. Experimenters were not blinded to group allocation during data collection.

Supporting Information

Supporting Information is available from the Wiley Online Library or from the author.

Acknowledgements

This research was funded by grants from the National Natural Science Foundation of China (82473163 to B.-A.L., 32371223 to H.G.), Fujian Provincial Natural Science Foundation of China (2024J01024 to H.G.), and Science and Technology Planning Projects of Xiamen (3502Z20224021 to W.L.). This work was also supported by the Postdoctoral Fellowship Program of CPSF (Grant No. GZC20231412) and the "Project 111" initiative, jointly sponsored by the State Bureau of Foreign Experts and the Ministry of Education (Grant No. B06016 to B.-A.L.).

Conflict of Interest

The authors declare no conflict of interest.

Author Contributions

S.W. and T.H. contributed equally to this work. S.W. designed the study, performed the majority of experiments, conducted data analysis, and drafted the manuscript. T.H., Y.Z., Y.-X.W., W.-L.X., T.F., and H.-M.S., contributed to mouse experiments. Y.L. conducted the bioinformatics analyses of RNA-seq. B.-A.L., H.-L.G., and W.-H.L. supervised the project, contributed to the manuscript revision, and provided funding. W.-H.L. acted as the guarantor, overseeing the study data, and is responsible for the integrity and accuracy of the data analysis.

Data Availability Statement

The data that support the findings of this study are available from the corresponding author upon reasonable request.

Ethics Statement

All mouse experiments were conducted in accordance with the guidelines of the Institutional Animal Care and Research Advisory Committee at Xiamen University, China, and were approved under Permit Number: XMULAC20230105.

Keywords

brown adipose tissue, mitochondrial biogenesis, metabolic disorders, SOX4, thermogenesis

Received: March 24, 2025
Revised: July 18, 2025
Published online:

[1] U. E. Bauer, P. A. Briss, R. A. Goodman, B. A. Bowman, *Lancet* **2014**, *384*, 45.
[2] G. Daryabor, M. R. Atashzar, D. Kabelitz, S. Meri, K. Kalantar, *Front. Immunol.* **2020**, *11*, 1582.
[3] G. Muscogiuri, L. Verde, C. Sulu, N. Katsiki, M. Hassapidou, E. Frias-Toral, G. Cucalón, A. Pazderska, V. D. Yumuk, A. Colao, L. Barrea, *Curr. Obes. Rep.* **2022**, *11*, 287.
[4] T. Baylie, T. Ayelgn, M. Tiruneh, K. H. Tesfa, *Diabetes Metab. Syndr. Obes.* **2024**, *17*, 1391.
[5] J H. Stern, J M. Rutkowski, P E. Scherer, *Cell Metab.* **2016**, *23*, 770.
[6] L. Cheng, J. Wang, H. Dai, Y. Duan, Y. An, L. Shi, Y. Lv, H. Li, C. Wang, Q. Ma, Y. Li, P. Li, H. Du, B. Zhao, *Adipocyte* **2021**, *10*, 48.
[7] B. Sahu, N. C. Bal, *Biochimie* **2023**, *204*, 92.
[8] B. Cannon, J. Nedergaard, *Physiol. Rev.* **2004**, *84*, 277.
[9] A. M. Cypess, S. Lehman, G. Williams, I. Tal, D. Rodman, A. B. Goldfine, F. C. Kuo, E. L. Palmer, Y. H. Tseng, A. Doria, G. M. Kolodny, C. R. Kahn, *N. Engl. J. Med.* **2009**, *360*, 1509.
[10] X. Wang, S.-Y. Liu, G.-S. Hu, H.-Y. Wang, G.-L. Zhang, X. Cen, S.-T. Xiang, W. Liu, P. Li, H. Ye, T.-J. Zhao, *Life Metab.* **2022**, *1*, 39.
[11] S. Rajakumari, J. Wu, J. Ishibashi, H. W. Lim, A. H. Giang, K. J. Won, R. R. Reed, P. Seale, *Cell Metab.* **2013**, *17*, 562.
[12] K. L. Marlatt, E. Ravussin, *Curr. Obes. Rep.* **2017**, *6*, 389.
[13] M. J. Harms, J. Ishibashi, W. Wang, H. W. Lim, S. Goyama, T. Sato, M. Kurokawa, K. J. Won, P. Seale, *Cell Metab.* **2014**, *19*, 593.
[14] L. Wu, M. Xia, Y. Duan, L. Zhang, H. Jiang, X. Hu, H. Yan, Y. Zhang, Y. Gu, H. Shi, J. Li, X. Gao, J. Li, *Cell Death Dis.* **2019**, *10*, 468.
[15] Y.-H. Lee, Y.-S. Jung, D. Choi, *Exp. Mol. Med.* **2014**, *46*, 78.
[16] A. M. Bertholet, Y. Kirichok, *Biochimie* **2017**, *134*, 28.
[17] Y. Lee, C. Willers, E. R. S. Kunji, P. G. Crichton, *Proc. Natl. Acad. Sci. USA* **2015**, *112*, 6973.
[18] M. Shi, X. Y. Huang, X. Y. Ren, X. Y. Wei, Y. Ma, Z. Z. Lin, D. T. Liu, L. Song, T. J. Zhao, G. Li, L. Yao, M. Zhu, C. Zhang, C. Xie, Y. Wu, H. M. Wu, L. P. Fan, J. Ou, Y. H. Zhan, S. Y. Lin, S. C. Lin, *Nat. Cell Biol.* **2021**, *23*, 268.
[19] C. B. Ueta, G. W. Fernandes, L. P. Capelo, T. L. Fonseca, F. D. Maculan, C. H. Gouveia, P. C. Brum, M. A. Christoffolete, M. S. Aoki, C. L. Lancellotti, B. Kim, A. C. Bianco, M. O. Ribeiro, *J. Endocrinol.* **2012**, *214*, 359.
[20] T. Pulinilkunnil, H. He, D. Kong, K. Asakura, O. D. Peroni, A. Lee, B. B. Kahn, *J. Biol. Chem.* **2011**, *286*, 8798.
[21] M. Harms, P. Seale, *Nat. Med.* **2013**, *19*, 1252.
[22] M. E. Symonds, *Scientifica (Cairo)* **2013**, *2013*, 305763.
[23] M. Uldry, W. Yang, J. St-Pierre, J. Lin, P. Seale, B. M. Spiegelman, *Cell Metab.* **2006**, *3*, 333.
[24] V. K. Mootha, C. Handschin, D. Arlow, X. Xie, J. St Pierre, S. Sihag, W. Yang, D. Altshuler, P. Puigserver, N. Patterson, P. J. Willy, I. G. Schulman, R. A. Heyman, E. S. Lander, B. M. Spiegelman, *Proc. Natl. Acad. Sci. USA* **2004**, *101*, 6570.
[25] M. J. Harms, H. W. Lim, Y. Ho, S. N. Shapira, J. Ishibashi, S. Rajakumari, D. J. Steger, M. A. Lazar, K. J. Won, P. Seale, *Genes Dev.* **2015**, *29*, 298.
[26] W. Wang, M. Kissig, S. Rajakumari, L. Huang, H. W. Lim, K. J. Won, P. Seale, *Proc. Natl. Acad. Sci. USA* **2014**, *111*, 14466.

[27] A. R. Angueira, S. N. Shapira, J. Ishibashi, S. Sampat, J. Sostre-Colón, M. J. Emmett, P. M. Titchenell, M. A. Lazar, H. W. Lim, P. Seale, *Cell Rep.* **2020**, *30*, 2869.
[28] M. Cheung, M. Abu-Elmagd, H. Clevers, P. J. Scotting, *Brain Res. Mol. Brain Res.* **2000**, *79*, 180.
[29] P. Dy, A. Penzo-Méndez, H. Wang, C. E. Pedraza, W. B. Macklin, V. Lefebvre, *Nucleic Acids Res.* **2008**, *36*, 3101.
[30] M. E. Wilson, K. Y. Yang, A. Kalousova, J. Lau, Y. Kosaka, F. C. Lynn, J. Wang, C. Mrejen, V. Episkopou, H. C. Clevers, M. S. German, *Diabetes* **2005**, *54*, 3402.
[31] T. He, S. Wang, S. Li, H. Shen, L. Hou, Y. Liu, Y. Wei, F. Xie, Z. Zhang, Z. Zhao, C. Mo, H. Guo, Q. Huang, R. Zhang, D. Shen, B. Li, *iScience* **2023**, *26*, 106289.
[32] H. Shen, T. He, S. Wang, L. Hou, Y. Wei, Y. Liu, C. Mo, Z. Zhao, W. You, H. Guo, B. Li, *Theranostics* **2022**, *12*, 7699.
[33] S. Wang, T. He, Y. Luo, K. Ren, H. Shen, L. Hou, Y. Wei, T. Fu, W. Xie, P. Wang, J. Hu, Y. Zhu, Z. Huang, Q. Li, W. Li, H. Guo, B. Li, *Cell Death Differ.* **2024**, *32*, 447.
[34] P. J. Fernandez-Marcos, J. Auwerx, *Am. J. Clin. Nutr.* **2011**, *93*, 884S.
[35] R. K. Semple, V. C. Crowley, C. P. Sewter, M. Laudes, C. Christodoulides, R. V. Considine, A. Vidal-Puig, S. O'Rahilly, *Int. J. Obes. Relat. Metab. Disord.* **2004**, *28*, 176.
[36] H. J. Lee, J. Lee, M. J. Yang, Y. C. Kim, S. P. Hong, J. M. Kim, G. S. Hwang, G. Y. Koh, *Nat. Commun.* **2023**, *14*, 2754.
[37] P. Kotzbeck, A. Giordano, E. Mondini, I. Murano, I. Severi, W. Venema, M. P. Cecchini, E. E. Kershaw, G. Barbatelli, G. Haemmerle, R. Zechner, S. Cinti, *J. Lipid Res.* **2018**, *59*, 784.
[38] S. Becerril, J. Gómez-Ambrosi, M. Martín, R. Moncada, P. Sesma, M. A. Burrell, G. Frühbeck, *Histol. Histopathol.* **2013**, *28*, 1411.
[39] C. De Jonge, *Front. Biosci.* **1996**, *1*, d234.
[40] S. L. Gray, E. Dalla Nora, E. C. Backlund, M. Manieri, S. Virtue, R. C. Noland, S. O'Rahilly, R. N. Cortright, S. Cinti, B. Cannon, A. Vidal-Puig, *Endocrinology* **2006**, *147*, 5708.
[41] J. Ishibashi, P. Seale, *Temperature (Austin)* **2015**, *2*, 65.
[42] S. Shams, M. Amirinejad, S. Amani-Shalamzari, H. Rajabi, K. Suzuki, *Comp. Biochem. Physiol. B Biochem. Mol. Biol.* **2023**, *265*, 110834.
[43] K. E. Claflin, K. H. Flippo, A. I. Sullivan, M. C. Naber, B. Zhou, T. J. Neff, S. O. Jensen-Cody, M. J. Potthoff, *Mol. Metab.* **2022**, *55*, 101405.